Applied Numerical Mathematics 200 (2024) 453–465

Contents lists available at ScienceDirect

Applied Numerical Mathematics

journal homepage: www.elsevier.com/locate/apnum

A numerical comparison of Galerkin and Collocation Isogeometric approximations of acoustic wave problems

Elena Zampieri [a,*,1], Luca F. Pavarino [b,1]

[a] Department of Mathematics, Università di Milano, Via Saldini 50, 20133 Milano, Italy
[b] Department of Mathematics, Università di Pavia, Via Ferrata 5, 27100 Pavia, Italy

ARTICLE INFO

Article history:
Received 18 January 2023
Received in revised form 1 June 2023
Accepted 4 June 2023
Available online 8 June 2023

Keywords:
Acoustic waves
Absorbing boundary conditions
Isogeometric analysis
Collocation
Galerkin
Newmark method

ABSTRACT

We consider the Galerkin and Collocation Isogeometric approximations of the acoustic wave equation with absorbing boundary conditions, while the time discretization is based on second-order Newmark schemes. A numerical study investigates the properties of the two IGA methods as concerns stability thresholds, convergence errors, accuracy, computational time, and sparsity of the stiffness matrices varying the polynomial degree p, mesh size h, regularity k, and time step Δt. In order to compare the two IGA methods, we focus on two meaningful examples in the framework of wave propagation simulations: a test problem with an oscillatory exact solution having increasing wave number, and the propagation of two interfering Ricker wavelets. Numerical results show that the IGA Collocation method retains the convergence and stability properties of IGA Galerkin. In all examples considered, IGA Collocation is in general less accurate when we adopt the same choices of parameters p, k, h, and Δt. On the other hand, regarding the computational cost and the amount of memory required to achieve a given accuracy, we observe that the IGA Collocation method often outperforms the IGA Galerkin method, especially in the case of maximal regularity $k = p - 1$ with increasing NURBS degree p.

1. Introduction

In the last decades, an increasing number of works have focused on high-order simulations of propagation problems in geophysics, using spectral, spectral elements, and isogeometric discretizations; see, e.g., [3,10,11,21], and references therein. In this paper, we compare Galerkin and Collocation Isogeometric approximations in space for the acoustic wave equation with absorbing boundary conditions, whereas the time approximation is based on Newmark schemes. Absorbing boundary conditions provide a good mathematical representation to simulate wave propagation in infinite domains, by truncating the infinite domain into a finite one; see, e.g., [8,15,18,27]. Other choices of time advancing schemes would could also be considered. In this regard, a new family of high-order explicit generalized-α methods for hyperbolic problems has been recently proposed in [5], with the feature of dissipation control.

* Corresponding author.
E-mail addresses: elena.zampieri@unimi.it (E. Zampieri), luca.pavarinoi@unipv.it (L.F. Pavarino).
[1] This work was partially supported by the European Research Council through the FP7 Ideas Consolidator Grant *HIGEOM* n. 616563, by the Italian Ministry of Education, University and Research (MIUR) through the "Dipartimenti di Eccellenza Program 2018-22 - Dept. of Mathematics, University of Pavia", and by the Istituto Nazionale di Alta Matematica (INdAM - GNCS), Italy.

https://doi.org/10.1016/j.apnum.2023.06.001

The main idea underlying the numerical approximation of partial differential equations (PDEs) with Isogeometric Analysis (IGA) is the representation of the domain starting from a Computer Aided Design (CAD) characterization, typically associated with B-Splines and Non-Uniform Rational B-Splines (NURBS); see e.g. [2,4,6,9]. Following the IGA approach, we formulate the Galerkin approximation of PDEs using the B-spline and NURBS basis functions firstly introduced to represent the CAD geometry. When comparing IGA discretization to more classical finite difference and finite element methods, besides the exact geometric description of a wide set of domains and high order of accuracy, IGA enables a k-refinement in addition to the standard p- and hp-refinement of hp-finite and spectral elements, where we have denoted by p the polynomial degree of the piecewise polynomial basis functions, by h the mesh size, and by k the global regularity of the IGA basis function, that may increase proportionally to the degree p, up to the maximal regularity $k = p - 1$ [20]. Several studies of structural, acoustic, and wave propagation problems show that the IGA k-refinement is superior to finite element p-refinement; see e.g. [21,10,16]. Furthermore, in [17], they present a detailed comparison of spectral elements and Galerkin IGA, focusing on the order of convergence of the methods and the spectral properties of their stiffness and mass matrices.

In the framework of NURBS-based IGA, we have initially considered the Galerkin approach [36] based on the weak formulation of the acoustic wave equation. Then we have extended our study to the collocation IGA variant [37], consisting in imposing the model problem written in its strong form at a certain set of collocation nodes, with the aim to enhance the storage of stiffness and mass matrices and computational cost, still taking advantage of IGA geometrical flexibility and accuracy. We have considered for simplicity the well-known Greville abscissae as collocation points providing an $O(h^{p-1})$ convergence order for odd p and $O(h^p)$ for even p. Other choices of isogeometric collocation points have been proposed in order to improve the convergence order, see e.g. the recent review [30]. Among these choices there are the Demko abscissae [14], superconvergent (SC) points [1], Cauchy–Galerkin (CG) points [19], and alternating/clustered superconvergent (ASC/CSC) points [26].

In our previous works, we have investigated experimentally the convergence and stability properties of the two IGA-Newmark methods, together with their computational efficiency and matrix sparsity with respect to all the parameters of the numerical problem. In both cases, we have also provided the stability thresholds, showing the linear dependence of the maximum step size Δt on h and on $1/p$.

The main novelty of this paper is a direct numerical comparison of the two Galerkin and Collocation IGA methods with respect to convergence error, computational cost, and sparsity of the stiffness matrices. In the first tests, we study the errors with respect to the degree p and mesh size h. Numerical solutions are compared with known analytical ones for test problems with oscillatory solutions having increasing wave number, while in our previous papers we tested the two methods separately on wave problems with smoother solutions. Then we consider the propagation of a Ricker wavelet originating at points positioned at different locations of the domain. While in our previous papers we consider only the case of one Ricker wavelet, here we consider a more demanding test with two interfering wavelets and compare the time evolution of the discrete energy (L^2-norm) of the acoustic pressure for the same sets of parameters.

All the tests indicate that the IGA Collocation method retains the convergence and stability properties of IGA Galerkin discretizations of acoustic problems. Detailed comparisons of convergence properties, computational cost CPUTIME, and stiffness matrix sparsity show that IGA Collocation is in general less accurate when we adopt the same choices of parameters p, k, h and Δt, either for the test with oscillatory solution or with the Ricker wavelet. Nevertheless, if we consider the global computational cost of matrix assembly and time advancing procedure, and the matrix sparsity, we observe that the IGA Collocation method often outperforms the IGA Galerkin method, especially when we consider the case of maximal regularity $k = p - 1$ with increasing NURBS degree p, since it requires a lower global computational cost and a smaller amount of memory in order to achieve a given accuracy.

The outline of this paper is as follows: In Section 2, we recall the acoustic wave model problem with absorbing boundary conditions. In Section 3, we recall the Newmark time-marching scheme and basic notions of B-spline and NURBS, and their application to IGA Galerkin and Collocation discretization of the wave model problem. Finally, Section 4 reports the results of several numerical experiments in the plane investigating the stability and convergence properties, computational costs, and efficiency of the IGA Galerkin and IGA Collocation methods with respect to space and time discretization parameters.

2. The model problem and mathematical analysis

Let $\Omega = [0,1] \times [0,1]$ be the reference domain in the plane with boundary $\Gamma \equiv \partial\Omega$. We denote by $\mathbf{x} = (x_1, x_2)$ any point of Ω. The temporal interval is $(0, T)$, with $T > 0$ and t is the time variable. We consider the acoustic wave problem (see e.g., Junger and Feit [23] and Ihlenburg [22]):

$$\frac{\partial^2 u}{\partial t^2}(\mathbf{x}, t) - c_0 \Delta u(\mathbf{x}, t) = f(\mathbf{x}, t) \quad \text{in } \Omega \times (0, T), \tag{1}$$

with initial conditions

$$u(\mathbf{x}, 0) = u_0(\mathbf{x}), \qquad \frac{\partial u}{\partial t}(\mathbf{x}, 0) = u_1(\mathbf{x}) \qquad \text{in } \Omega, \tag{2}$$

and absorbing boundary conditions on the whole boundary Γ

$$\frac{1}{\sqrt{c_0}}\frac{\partial u}{\partial t}(\mathbf{x},t)+\frac{\partial u}{\partial \mathbf{n}}(\mathbf{x},t)=g(\mathbf{x},t) \qquad \text{on } \Gamma\times(0,T). \tag{3}$$

In the above equations u is the unknown acoustic pressure, c_0 is the acoustic wave propagation velocity, f is the source term, u_0 and u_1 are the initial pressure and velocity, respectively.

Absorbing Boundary Conditions (3) (ABCs for brevity) are frequently used for the numerical simulation of acoustic or elastic wave problems in infinite domains, see [8,15,27,18,29]. The given unbounded domain is truncated into a finite domain, then ABCs are imposed on the artificial boundaries of the truncated domain in order to keep spurious wave reflections as low as possible, making the boundary transparent to outgoing and opaque to incoming waves. Even if it would be possible to enforce exact transmitting boundary conditions, these would be non-local in both space and time, therefore difficult to use in numerical computations. Natural first-order ABCs involve first spatial and temporal partial derivatives only, with $g=0$ on Γ. In (3) ABCs have been properly modified by assigning a suitable function $g\in L^2(\Gamma\times(0,T))$ in order to investigate the convergence error of the numerical solutions with respect to the exact ones (see Section 4). The source term g and the partial derivative $\partial\cdot/\partial t$ are thus dealt with as a boundary load associated with a standard Neumann condition.

For possible extensions with higher-order ABCs involving also derivatives of order greater than one, as well as derivatives in the tangential direction, we refer e.g. to [18].

The corresponding variational formulation of (1)-(3) reads as follows:

Find $u:(0,T)\to H^1(\Omega)$, such that for *a.e.* $t\in(0,T)$:

$$\left(\frac{\partial^2 u}{\partial t^2},v\right)+a(u,v)+\sqrt{c_0}<\frac{\partial u}{\partial t},v>_\Gamma=(f,v)+<g,v>_\Gamma \quad \forall v\in H^1(\Omega), \tag{4}$$

where

$$a(u,v)=c_0\int_\Omega \nabla u\cdot\nabla v\,\mathrm{d}x_1\mathrm{d}x_2, \quad (f,v)=\int_\Omega f v\,\mathrm{d}x_1\mathrm{d}x_2, \quad <\frac{\partial u}{\partial t},v>_\Gamma=\int_\Gamma \frac{\partial u}{\partial t}v\,\mathrm{d}s.$$

The stability of the continuous acoustic problem can be proved following the analysis that has been carried out in Quarteroni, Tagliani and Zampieri [29] for elastodynamics linear problems.

3. Discretization of the acoustic wave problem

We briefly describe the numerical approximation of the acoustic wave problem, in the weak (4) and strong (1)-(3) forms, respectively. The temporal discretization is based on Newmark's time advancing schemes, whereas the spatial approximation is based on IGA Galerkin and Collocation.

3.1. Newmark time advancing schemes

For the approximation of time derivatives we consider the finite difference Newmark schemes. We subdivide the temporal interval $[0,T]$ into N subintervals $[t_{n-1},t_n]$, with $t_0=0$, $t_N=T$, $\Delta t=T/N$, $t_n=n\Delta t$, $n=1,\ldots,N-1$. The Newmark method [28] in its general form reads:

$$\mathbf{u}_{n+1}=\mathbf{u}_n+\Delta t\,\mathbf{v}_n+(1-2\beta)\Delta t^2\mathbf{a}_n/2+\beta\Delta t^2\mathbf{a}_{n+1},\ \mathbf{v}_{n+1}=\mathbf{v}_n+(1-\gamma)\Delta t\,\mathbf{a}_n+\gamma\Delta t\mathbf{a}_{n+1}, \tag{5}$$

where $\mathbf{u}_n$, $\mathbf{v}_n$, $\mathbf{a}_n$ are the vectors of approximated displacement, velocity and acceleration values at nodal points, respectively, and at time t_n, with $\beta\geq 0$ and $\gamma\geq 0$ real parameters. It can be shown that the Newmark scheme can be expressed as a two-step algorithm in the displacement only, by eliminating the velocity and acceleration terms (see, e.g., [34], [35]). In Sections 3.3 and 3.4 it is applied to IGA Galerkin and Collocation approximation of the wave equation, respectively. We remark that other choices of time advancing schemes would be possible. For instance, a new family of high-order explicit k-step generalized-α methods for hyperbolic problems has been recently proposed in [5], providing $2k$ order of accuracy in time and improved dissipation properties.

3.2. B-splines and NURBS-based Isogeometric Analysis

Given a *knot vector* on the reference interval of non-decreasing real numbers

$$\{\xi_1=0,\ldots,\xi_{\nu+p+1}=1\}, \tag{6}$$

where p is the polynomial degree and ν is the number of basis functions and control points of the B-spline, respectively, the univariate B-spline basis functions are built recursively and denoted by N_i^p, with support (ξ_i,ξ_{i+p+1}), $i=1,2,\ldots,\nu$ (see, e.g. [31]). We recall that B-spline basis functions are C^{p-1}-continuous if internal nodes are not repeated, whereas they are C^k-continuous, with $k=p-\alpha$, if the associated knot has multiplicity equal to α. In particular, when a knot has multiplicity $\alpha=p$, the basis is C^0-continuous, interpolating the control point at that location where the knot has multiplicity α. From

now on, we will assume that the maximum knot multiplicity is p ensuring that all considered functions are at least globally continuous. For the simplicity of exposition, here we examine the case of B-spline of same degree p in each directions. Then, we introduce the two-dimensional parametric space $\widehat{\Omega} := (0,1) \times (0,1)$ with a knot vector (6) in each direction, and $\mathbf{C}_{i,j}$ is a net of ν^2 control points, $i, j = 1, ..., \nu$. The case of higher-dimensional case and different degrees can be dealt with analogously.

Given the one-dimensional spline space:

$$\text{span}\{N_i^p(\xi), i = 1, \dots, \nu\},$$

we build the multi-dimensional B-spline basis functions on $\widehat{\Omega}$ by tensor product as $B_{i,j}^p(\xi,\eta) = N_i^p(\xi)N_j^p(\eta)$. Similarly, the mesh of rectangular elements in the parametric space is generated in a natural way by the Cartesian product of two knot vectors $\{\xi_1 = 0, ..., \xi_{\nu+p+1} = 1\}$, and

$$\widehat{\mathcal{S}}_h = \text{span}\{B_{i,j}^p(\xi,\eta),\ i, j = 1, \dots, \nu\} \tag{7}$$

is the bi-variate spline space. We recall that a rational B-spline in $\mathbb{R}^d$ is obtained by projecting onto d-dimensional physical space a polynomial B-spline assigned in $(d+1)$-dimensional homogeneous coordinate space. We indicate a NURBS basis function of degree p as

$$R_i^p(\xi) = \frac{N_i^p(\xi)\omega_i}{\sum_{\hat{i}=1}^{\nu} N_{\hat{i}}^p(\xi)\omega_{\hat{i}}} = \frac{N_i^p(\xi)\omega_i}{w(\xi)}, \tag{8}$$

where $w(\xi) = \sum_{\hat{i}=1}^{\nu} N_{\hat{i}}^p(\xi)\omega_{\hat{i}} \in \widehat{\mathcal{S}}_h$ is a weight function. Analogously to the construction of B-splines, NURBS basis functions on the two-dimensional parametric space $\widehat{\Omega}$ are constructed from the bi-variate spline basis as

$$R_{i,j}^p(\xi,\eta) = \frac{B_{i,j}^p(\xi,\eta)\omega_{i,j}}{\sum_{\hat{i},\hat{j}=1}^{\nu} B_{\hat{i},\hat{j}}^p(\xi,\eta)\omega_{\hat{i},\hat{j}}} = \frac{B_{i,j}^p(\xi,\eta)\omega_{i,j}}{w(\xi,\eta)}, \tag{9}$$

where $\omega_{i,j} \in \mathbb{R}$, and the denominator is the two-dimensional weight function. NURBS basis functions have the same continuity and support of B-splines, and the span of the basis functions (9) provides NURBS spaces in a similar way. Let us consider a *single-patch* domain Ω as a NURBS region associated with the net $\mathbf{C}_{i,j}$. We introduce the geometrical map $\mathbf{F} : \widehat{\Omega} \to \Omega$ defined by

$$\mathbf{F}(\xi,\eta) = \sum_{i,j=1}^{\nu} R_{i,j}^p(\xi,\eta)\mathbf{C}_{i,j}. \tag{10}$$

According to the isoparametric IGA approach the span of the *push-forward* of the basis functions (9) yields the space of NURBS scalar fields on the domain Ω is defined by the isoparametric approach as

$$\mathcal{N}_h := \text{span}\{R_{i,j}^p \circ \mathbf{F}^{-1},\ \text{with } i, j = 1, \dots, \nu\}. \tag{11}$$

3.3. IGA Galerkin discretization of the acoustic problem

We consider the variational form of the acoustic wave problem (4) and replace the L^2-inner products and the bilinear form with their IGA quadrature-based approximations. The semidiscrete continuous-in-time problem reads: For each $t \in (0,T)$, find $u_h \in \mathcal{N}_h$ such that:

$$\left(\frac{\partial^2 u_h}{\partial t^2}, v\right)_h + a_h(u_h, v) + \sqrt{c_0} < \frac{\partial u_h}{\partial t}, v >_{h,\Gamma} = (f, v)_h + < g, v >_{h,\Gamma} \quad \forall v \in \mathcal{N}_h, \tag{12}$$

where $(\cdot,\cdot)_h$, $a_h(\cdot,\cdot)$, $< \cdot, \cdot >_{h,\Gamma}$ are the IGA L^2-quadrature, stiffness and boundary bilinear forms, respectively. The algebraic form of problem (12) is obtained by expanding both the solution and the test functions using the IGA basis functions, thus providing a system of second-order ordinary differential equations [36]

$$\mathcal{M}\ddot{\mathbf{u}}(t) + \mathcal{C}\dot{\mathbf{u}}(t) + \mathcal{K}\mathbf{u}(t) = \mathbf{F}(t) + \mathbf{G}(t), \tag{13}$$

with initial conditions $\mathbf{u}(0) = \mathbf{u}_0$, $\dot{\mathbf{u}}(0) = \mathbf{u}_1$. In system (13) $\mathcal{K}$ and $\mathcal{M}$ are the assembled stiffness and mass IGA matrices, respectively, whereas $\mathcal{C}$ accounts for first-order time derivatives at nodes of Γ. We recall that $\mathcal{M}$, $\mathcal{C}$ and $\mathcal{K}$ are symmetric, $\mathcal{M}$ is positive definite, whereas $\mathcal{K}$ is symmetric and positive semi-definite. The matrix $\mathcal{C}$ is positive semi-definite with most elements equal to zero. Finally, $\forall t \in (0,T)$, $\mathbf{u}(t)$ is the vector of coefficients of u_h in the IGA basis, $\mathbf{F}(t)$ and $\mathbf{G}(t)$ are

known vectors accounting for the contribution of f and g, respectively. If we denote by $\Upsilon(t)$ the right-hand side of (13), the application of the Newmark scheme (5) to (13) gives the recurrence relations:

$$\mathcal{M}\frac{\mathbf{u}_{n+1}-2\mathbf{u}_n+\mathbf{u}_{n-1}}{\Delta t^2}+\mathcal{C}\frac{\gamma\mathbf{u}_{n+1}+(1-2\gamma)\mathbf{u}_n+(\gamma-1)\mathbf{u}_{n-1}}{\Delta t}+$$
$$\mathcal{K}\Big[\beta\mathbf{u}_{n+1}+\Big(\frac{1}{2}-2\beta+\gamma\Big)\mathbf{u}_n+\Big(\frac{1}{2}+\beta-\gamma\Big)\mathbf{u}_{n-1}\Big]=\Big[\beta\Upsilon_{n+1}+\Big(\frac{1}{2}-2\beta+\gamma\Big)\Upsilon_n+\Big(\frac{1}{2}+\beta-\gamma\Big)\Upsilon_{n-1}\Big]. \quad (14)$$

3.4. IGA Collocation discretization of the acoustic problem

In this section we briefly review the IGA collocation method, see [2,3,32], and apply it to our acoustic wave problem, having chosen the Greville abscissae associated to the knot vectors as collocation points, see [13]. We remark that in addition to the well-known Greville points, other choices of isogeometric collocation points have been proposed, see e.g. the recent review [30]. Among these choices there are the Demko abscissae [14], superconvergent (SC) points [1], Cauchy–Galerkin (CG) points [19], and alternating/clustered superconvergent (ASC/CSC) points [26]. Demko and Greville points share an $O(h^{p-1})$ convergence order for odd p and $O(h^p)$ for even p. SC and ASC/CSC points improve the convergence order to $O(h^{p+1})$ for odd p, but retain an $O(h^p)$ order for even p. CG points have $O(h^p)$ convergence order for both odd and even degrees p. In this work, we will consider for simplicity the Greville points.

Let $\overline{\xi}_i$, $i=1,...,\nu$, be the Greville nodes associated to the given knot vector (6):

$$\overline{\xi}_i \doteq (\xi_{i+1}+\xi_{i+2}+...+\xi_{i+p})/p\,, \quad (15)$$

where $\overline{\xi}_1=0$, $\overline{\xi}_n=1$, and the remaining points are in $(0,1)$. The grid of collocation points $\tau_{ij}\in\Omega$ is defined by the tensor product

$$\tau_{ij}=\mathbf{F}(\widehat{\tau}_{ij})\,, \qquad \widehat{\tau}_{ij}=(\overline{\xi}_i,\overline{\xi}_j)\ \in\ \overline{(\widehat{\Omega})}\,,\ \ i,j=1,...,\nu.$$

The theory of the IGA collocation method for elliptic problems in two and three dimensions still has many open issues; despite the lack of proven results, several numerical tests in the literature exhibit the stability and convergence of the method in a large number of practical cases.

In order to describe the collocation problem, we enumerate the grid points $\{\tau_{ij}\}$ using only one index. Each collocation point $\tau_{ij}\in\Omega$, $i,j=1,...,\nu$, is thus associated to the point P_k of the tensor product grid, with $k=1,...,\nu^2$. Then we define two disjoint sets of indexes $\mathcal{I}_\Omega:=\{k|P_k\in\Omega\}$ and $\mathcal{I}_\Gamma:=\{k|P_k\in\Gamma\}$, associated to internal and boundary points, respectively. We denote by $\mathcal{I}:=\mathcal{I}_\Omega\cup\mathcal{I}_\Gamma$ the set of ν^2 indexes of the whole grid of mesh points. The IGA collocation semi-discrete continuous-in-time formulation of the acoustic problem (1)-(3) is obtained by collocating the continuous problem at the Greville collocation points:

$$\frac{\partial^2 u}{\partial t^2}(P_k,t)-c_0\Delta u(P_k,t)=f(P_k,t),\quad k\in\mathcal{I}_\Omega,\ t\in(0,T), \quad (16)$$

with initial conditions

$$u(P_k,0)=u_0(P_k),\qquad \frac{\partial u}{\partial t}(P_k,0)=u_1(P_k),\qquad k\in\mathcal{I}, \quad (17)$$

and ABCs

$$\frac{1}{\sqrt{c_0}}\frac{\partial u}{\partial t}(P_k,t)+\frac{\partial u}{\partial \mathbf{n}}(P_k,t)=g(P_k,t),\qquad k\in\mathcal{I}_\Gamma,\ t\in(0,T). \quad (18)$$

The semi-discrete collocation problem is equivalent to the problem of finding a vector $\mathbf{u}$ of elements $\{u_k,\ k\in\mathcal{I}\}$, in correspondence with elements $\{u_{ij},\ i,j=1,...,\nu^2\}$ providing the IGA numerical solution

$$u(\mathbf{x},t)=\sum_{i=1}^{\nu}\sum_{j=1}^{m}u_{ij}R_{ij}^{p,q}\circ\mathbf{F}^{-1}(\mathbf{x},t), \quad (19)$$

according to (10) and (11). We introduce now the IGA collocation matrices $[D_r]$, with $r=0,\ 1,\ 2$, accounting for r-th derivatives at collocation points, where D_0, D_1 and D_2 are associated to the identity, $\frac{\partial}{\partial\mathbf{n}}$ and Δ operators, respectively. The precise MATLAB construction is based on the structure `sp_eval` of the GeoPDEs library [12]. Equations (16)-(18) can be then rewritten in matrix form as a system of second-order ordinary differential equations [37]:

$$\frac{\partial^2}{\partial t^2}[D_0\mathbf{u}(t)]_k-c_0[D_2\mathbf{u}(t)]_k=[\mathbf{f}(t)]_k,\ k\in\mathcal{I}_\Omega,\quad \frac{1}{\sqrt{c_0}}\frac{\partial u}{\partial t}[D_0\mathbf{u}(t)]_k+[D_1\mathbf{u}(t)]_k=[\mathbf{g}(t)]_k,\ k\in\mathcal{I}_\Gamma, \quad (20)$$

$$[D_0\mathbf{u}(0)]_k=[\mathbf{u}_0]_k,\quad \frac{\partial}{\partial t}[D_0\mathbf{u}(0)]_k=[\mathbf{u}_1]_k,\quad k\in\mathcal{I}, \quad (21)$$

where $\mathbf{u}(t) := [u(P_k,t)],\ k\in\mathcal{I}$, $\mathbf{f}(t) := [f(P_k,t)],\ k\in\mathcal{I}$, $\mathbf{g}(t) := [g(P_k,t)],\ k\in\mathcal{I}_\Gamma$, $\mathbf{u}_0 := [u_0(P_k)],\ k\in\mathcal{I}$, $\mathbf{u}_1 := [u_1(P_k)],\ k\in\mathcal{I}$, and all vectors are assigned equal to zero elsewhere.

When the Newmark scheme (5) is applied to the numerical solution of the acoustic wave IGA collocation problem (20)-(21), if we denote by $[D_r]_k$ the k-th row of the collocation matrix D_r, $r=0,1,2$, and by $[\mathbf{w}]_k$ the k-th element of a general vector $\mathbf{w}$, we obtain the set of recurrence relations at collocation points:

$$[D_0]_k\frac{\mathbf{u}_{n+1}-2\mathbf{u}_n+\mathbf{u}_{n-1}}{\Delta t^2}-c_0[D_2]_k\Big[\beta\mathbf{u}_{n+1}+\Big(\frac{1}{2}-2\beta+\gamma\Big)\mathbf{u}_n+\Big(\frac{1}{2}+\beta-\gamma\Big)\mathbf{u}_{n-1}\Big]= \tag{22}$$
$$\Big[\beta\mathbf{f}_{n+1}+\Big(\frac{1}{2}-2\beta+\gamma\Big)\mathbf{f}_n+\Big(\frac{1}{2}+\beta-\gamma\Big)\mathbf{f}_{n-1}\Big]_k,\quad k\in\mathcal{I}_\Omega,$$
$$\frac{1}{\sqrt{c_0}}[D_0]_k\frac{\gamma\mathbf{u}_{n+1}+(1-2\gamma)\mathbf{u}_n+(\gamma-1)\mathbf{u}_{n-1}}{\Delta t}+[D_1]_k\mathbf{u}_{n+1}=[\mathbf{g}_{n+1}]_k,\quad k\in\mathcal{I}_\Gamma. \tag{23}$$

At any corner point involving ABCs we enforce the average of normal derivatives.

Remark 1. By using Taylor expansions it can be proven that the Newmark method is first-order accurate with respect to Δt if $\gamma\neq\frac{1}{2}$, and it is second-order if $\gamma=\frac{1}{2}$. The schemes (14) and (22)-(23) are explicit if $\beta=0$ and coincide with the *Leap-Frog* method when $\gamma=\frac{1}{2}$, which in particular is explicit and second-order accurate with respect to Δt. Nevertheless, the IGA matrices associated to Galerkin (14) and Collocation (16)-(18) approximations are full both for explicit ($\beta=0$) and implicit ($\beta\neq0$) case, since the corresponding IGA mass matrices are not diagonal. Therefore, each step of either the explicit or the implicit method involves the resolution of a linear system, possibly involving effective preconditioning techniques (e.g., [24]). See [36] and [37] for details.

Remark 2. The required second initial vector $\mathbf{u}_1$ can be computed from the first one $\mathbf{u}_0$ associated to initial condition (2)-left applying a second-order explicit one-step method, e.g., an explicit two-stage Runge-Kutta method, thus preserving the global accuracy of the numerical scheme with respect to the time step Δt, and using (2)-right.

4. Numerical results

In this Section we present the numerical tests for the acoustic wave problem with absorbing boundary conditions (2)-(3), discretized in time with the Newmark scheme of Sec. 3.1, and in space with the IGA Galerkin (IGA-Gal) of Sec. 3.3 and the IGA collocation methods (IGA-Col) of Sec. 3.4. We will focus on the stability and convergence properties of the two methods, as functions of the parameters polynomial degree p, mesh size h, regularity k and time step Δt. All tests refer to the reference square domain $\Omega=[0,1]\times[0,1]$, Newmark parameters $\beta=0$ and $\gamma=0.5$ and are implemented in MATLAB R2020b by the GeoPDEs library [12,33], within a 64-bit Intel(R) Core(TM) i5-10210U CPU up to 2.10 GHz with 8 GB of RAM. For several tests considering also non Cartesian domains and different choices of the Newmark parameters see [36] and [37]. (For a complete interpretation of the color figures and comments reported in this Section, the reader is referred to the web version of this article.)

In the first tests the right-hand sides f, g and initial conditions u_0 and u_1 are assigned in such a way that the exact solution of the wave problem (2)-(3) is given by

$$u(\mathbf{x},t)=\sin(m\pi x_1)\sin(m\pi x_2)\sin(t),\ m\in\mathbb{N}. \tag{24}$$

For each time step t_n we compare the exact solution (24) with the IGA-Newmark solutions using the `sp_l2_error` function of the GeoPDEs library [12], according to which the errors $e(p,h,\Delta t)$ are obtained evaluating the discrete L^2-norm of the difference between the exact and the IGA-Gal and IGA-Col solutions.

In the last examples we will consider instead a source f given by a Ricker wavelet placed at one or two given points of the square Ω, with g, u_0 and u_1 equal to zero.

Stability. In Fig. 1 we plot the Δt stability thresholds as a function of h (left panel) for fixed $p=5$, $k=4$, and as a function of p (right panel) for fixed $1/h=10$, $k=p-1$. The test function is given by (24), with $m=1$. The stability thresholds seem to be linear in h for fixed p, and linear in $1/p$ for fixed h, and $k=p-1$ in both panels. Moreover, the maximal Δt that guarantees stability in the case of IGA-Col are at least twice the IGA-Gal thresholds, showing less restrictive stability constraints than in the case of the IGA-Gal method.

Accuracy: oscillatory solution. Table 1 reports the errors $e(p,h,\Delta t)$, with time step $\Delta t=0.001$ at time $t_n=1$, as a function of p, for fixed mesh size $1/h=4$ and maximal regularity $k=p-1$ for different values of $m=1,2,4,6$ in the test function (24), in order to compare the accuracy of IGA-Gal (left table) and IGA-Col (right table) in dealing with an exact solution presenting increasing wave numbers. Results show that the accuracy is similar for highly oscillatory solutions, whereas the IGA-Gal performs better than the IGA-Col for smaller values of m.

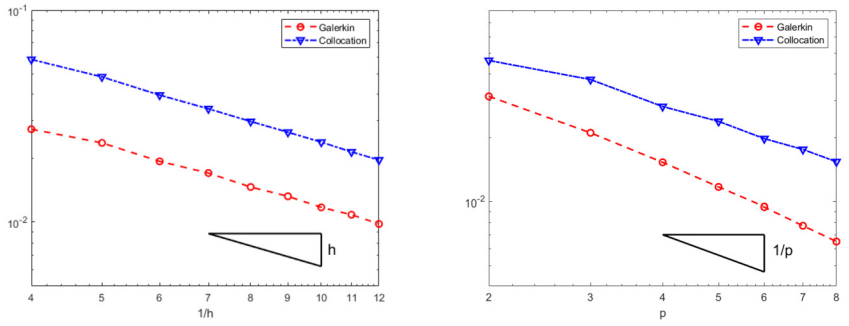

Fig. 1. Δt stability thresholds vs h (left) for fixed $p = 5,\ k = 4$ (left) and vs p for fixed $1/h = 10,\ k = p - 1$ (right), for IGA-Gal (dashed lines) and IGA-Col (continuous lines).

Table 1
Error $e(p, h, \Delta t)$ vs p, for $k = p - 1,\ 1/h = 4,\ \Delta t = 0.001$ and different values of $m = 1, 2, 4, 6$ in the test function (24), for IGA-Gal (left) and IGA-Col (right).

p	$m=1$	$m=2$	$m=4$	$m=6$	$m=1$	$m=2$	$m=4$	$m=6$
	Galerkin				Collocation			
3	2.575e-4	7.133e-3	2.303e-1	4.219e-1	3.599e-2	8.161e-2	8.389e-1	1.728e-0
4	3.285e-5	1.211e-3	2.689e-3	2.789e-1	5.632e-4	1.255e-2	3.920e-2	2.039e-0
5	4.256e-6	6.152e-4	6.212e-2	3.623e-1	1.341e-4	1.445e-3	1.544e-1	7.112e-1
6	5.613e-7	1.337e-5	2.526e-4	9.834e-2	3.306e-6	5.069e-4	8.454e-4	2.622e-1
7	4.217e-8	2.690e-5	9.777e-3	1.664e-1	1.020e-6	1.829e-4	4.580e-2	2.807e-1
8	6.070e-9	1.397e-6	2.693e-5	2.202e-2	1.064e-7	4.721e-5	2.657e-5	3.460e-2

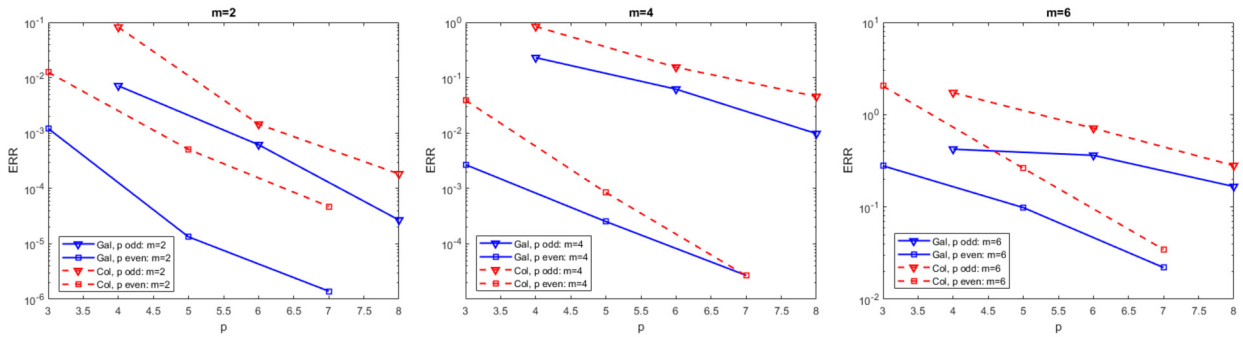

Fig. 2. Error $e(p, h, \Delta t)$ vs odd values of p (triangles) and even values of p (squares), for $k = p - 1,\ 1/h = 4,\ \Delta t = 0.001$ and $m = 2$ (left), $m = 4$ (center), $m = 6$ (right) in the test function (24), for IGA-Gal (blue continuous lines) and IGA-Col (red dashed lines).

In Fig. 2 we report the same data as in Table 1, for the cases $m = 2$ (left) $m = 4$ (center), $m = 6$ (right), by separating odd (triangle markers) and even (square markers) values of p, for IGA-Gal (blue continuous lines) and IGA-Col (red dashed lines). Again, if we fix the same set of discretization parameters, we observe the better accuracy of IGA-Gal with respect to IGA-Col method. We also observe that the convergence rates in p are similar but the errors are better for even values of polynomial degree p than for odd values, since the continuous lines are definitely below the dashed ones. With regard to this different behavior for even and odd degrees p, the problem of removing spurious outliers in the Laplacian's eigenvalues corresponding to even or odd values of degree p has been recently dealt with in the framework of IGA Galerkin approximation in [25].

Convergence and CPU TIME. We compare now the computational costs CPUTIME - including initialization and assembly operations until the end of the time advancing procedures - and convergence errors $e(p, h, \Delta t)$ computed at time t_n of IGA-Gal (continuous lines) and IGa-Col (dashed lines). Numerical results refer to exact solutions (24) with $m = 1$ and time step $\Delta t = 0.001$. Fig. 3 shows from the top to the bottom: the errors versus the mesh size h (1), CPUTIME (2), degrees of freedom dofs (3), and CPUTIME versus dofs (4). We consider four different values of degree p and minimal regularity $k = 1$ (left) or three different values of degree p and maximal regularity $k = p - 1$ (right).

In Fig. 4 we report results analogous to those of Fig. 3, but now we vary the degree p and consider three different values of the mesh size h. The IGA-Gal simulations are definitely more accurate than IGA-Col ones when we adopt the same set of discretization parameters both for increasing $1/h$ with fixed p and for increasing p with fixed $1/h$. As a matter of fact we observe that IGA-Gal errors are 3-4 orders of magnitude smaller than the analogous IGA-Col ones. In the case of maximal

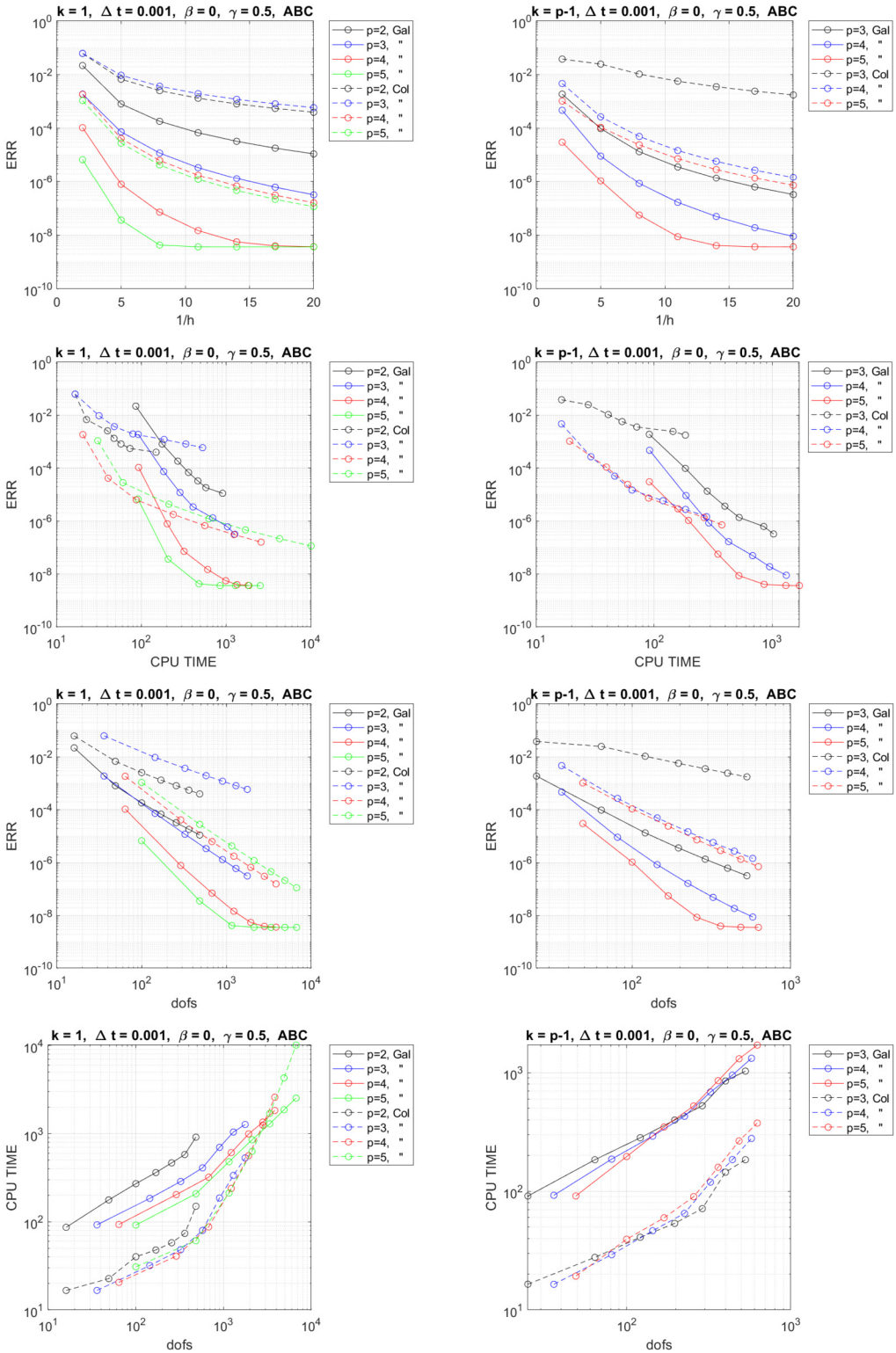

Fig. 3. Accuracy and CPUTIME of IGA-New-Gal (continuous lines) and IGA-New-Col (dashed lines) as a function of the mesh size h fixed $p = 2, 3, 4, 5$ on the left panel with regularity $k = 1$ and $p = 3, 4, 5$ on the right panel with regularity $k = p - 1$. From the top to the bottom: errors versus the mesh size h (1), CPUTIME (2), degrees of freedom dofs (3), and CPUTIME versus dofs (4). Test function (24) with $m = 1$, $\Delta t = 0.001$.

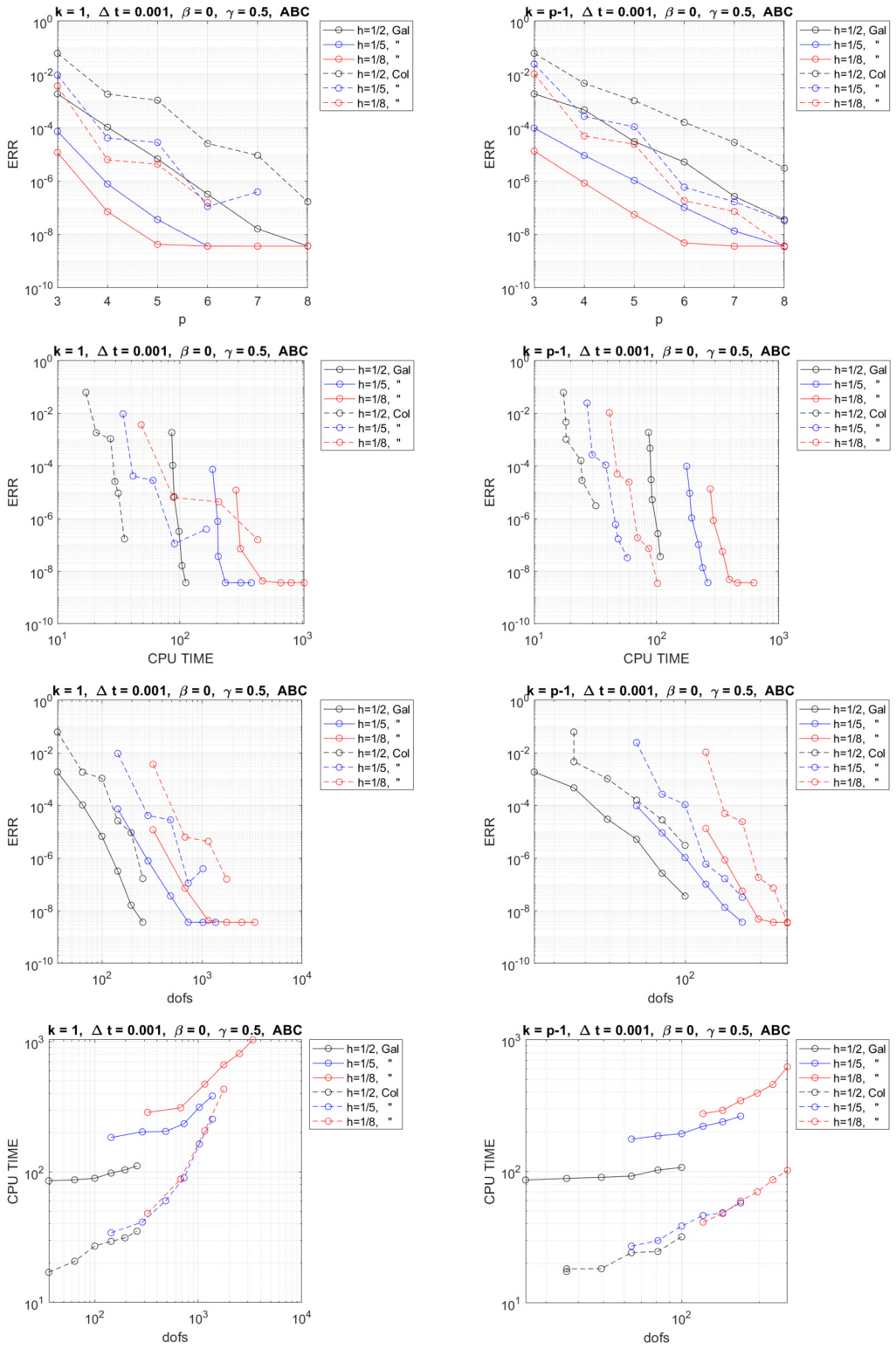

Fig. 4. Accuracy and CPUTIME of IGA-New-Gal (continuous lines) and IGA-New-Col (dashed lines) as a function of the degree p fixed $1/h = 2, 5, 8$ with regularity $k = 1$ (left panel) and with regularity $k = p - 1$ (right panel). From the top to the bottom: errors versus the degree p (1), CPUTIME (2), degrees of freedom dofs (3), and CPUTIME versus dofs (4), with regularity $k = 1$ (left) or $k = p - 1$ (right). Test function (24) with $m = 1$, $\Delta t = 0.001$.

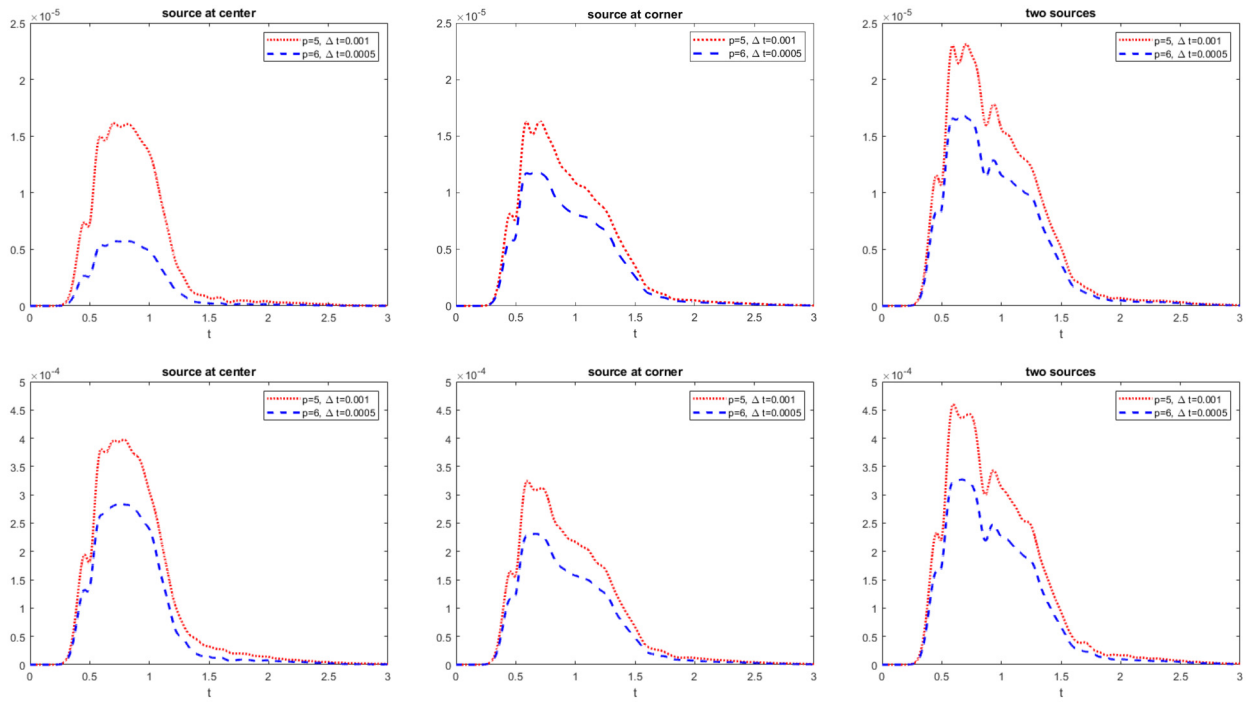

Fig. 5. Time evolution on the interval $[0,\ 3]$ of the energy (L_2-norm) of the numerical solution: one Ricker wavelet located at the center of the square domain (left); one Ricker wavelet located near the corner of the square domain (center); two Ricker wavelets located near the corners of the square domain (right). B-splines with $p=5,\ k=4$, $h=1/8$ and $\Delta t=0.001$ (red dotted lines) or with $p=6,\ k=5$, $h=1/10$ and $\Delta t=0.0005$ (blue dashed lines), for the IGA-Gal (top panel) and the IGA-Col (bottom panel) variants.

regularity the errors are still smaller but with a reduced gap of 1-2 orders of magnitude. Alternative considerations can be made if we compare the CPUTIME of IGA-Gal and IGA-Col versus dofs, since the dashed collocation lines are definitely in the bottom part of the figures showing that using IGA-Col methods it can be reached a given error value in a smaller CPUTIME with respect to the IGA-Gal variant. This behavior is even clearer in the case of maximal regularity $k=p-1$ (right panel).

Ricker wavelet tests. As final tests we consider the propagation of one Ricker wavelet originating first at a point P located either at the center $P_1(0.5,0.5)$ or at $P_2(2/9,2/9)$ near the corner of the square domain Ω, and finally of two Ricker wavelets located at P_2 and at its symmetric $P_2'(1-2/9,1-2/9)$ with respect to the center of the domain, thus considering a more demanding test taking into account the effect of interference of two sources. In all cases we set homogeneous initial conditions in (2). We recall that according to the expression of the Ricker wavelet the source is given by

$$f(\mathbf{x},t)=\begin{cases}\left[2\tilde{f}(t-t_0)^2-1\right]e^{-\tilde{f}(t-t_0)^2} & \mathbf{x}=P\\ 0 & \text{elsewhere}\end{cases} \tag{25}$$

where we have fixed $\tilde{f}=100$ and $t_0=0.5$. Fig. 5 displays the time evolution of the Ricker wavelet L^2-norm for the IGA-Gal (top panel) and for the IGA-Col (bottom panel) in the three tests with source term given by: one wavelet located at the center P_1 of the square domain (left), one wavelet located at P_2, near one corner of the square domain (center), and two wavelets located at P_2 and at P_2' near two opposite corners of the domain (right). The numerical discretization consists of B-splines with $p=5,\ k=4$, mesh size $h=1/8$ and time step $\Delta t=0.001$ (red dotted lines) or with $p=6,\ k=5$, mesh size $h=1/10$ and time step $\Delta t=0.0005$ (blue dashed lines). We observe that the L^2-norm curves are qualitative similar in each of the three cases for the two IGA variants, with a decrease of the pressure toward zero for $t>1$. Nonetheless, the performance of the IGA-Gal simulation is more accurate yielding values of L^2- energy that are one order of magnitude smaller than in the corresponding IGA-Col case.

Finally, the propagation of the wavelet is also displayed in Fig. 6 for the IGA-Gal with the Ricker wavelet source located at $P\equiv P_2$, and in Fig. 7 for the IGA-Col with two Ricker wavelet sources located at $P\equiv P_2$ and $P\equiv P_2'$. We show nine representative snapshots of the pressure field u at times $t=0.25,0.50,0.75,1.00,1.25,1.50,1.750,2.00,3$, fixed $p=6,\ k=5$, mesh size $h=1/10$ and $\Delta t=0.0005$. In both cases the pulses dissipate across the absorbing domain boundaries with negligible spurious wave reflections.

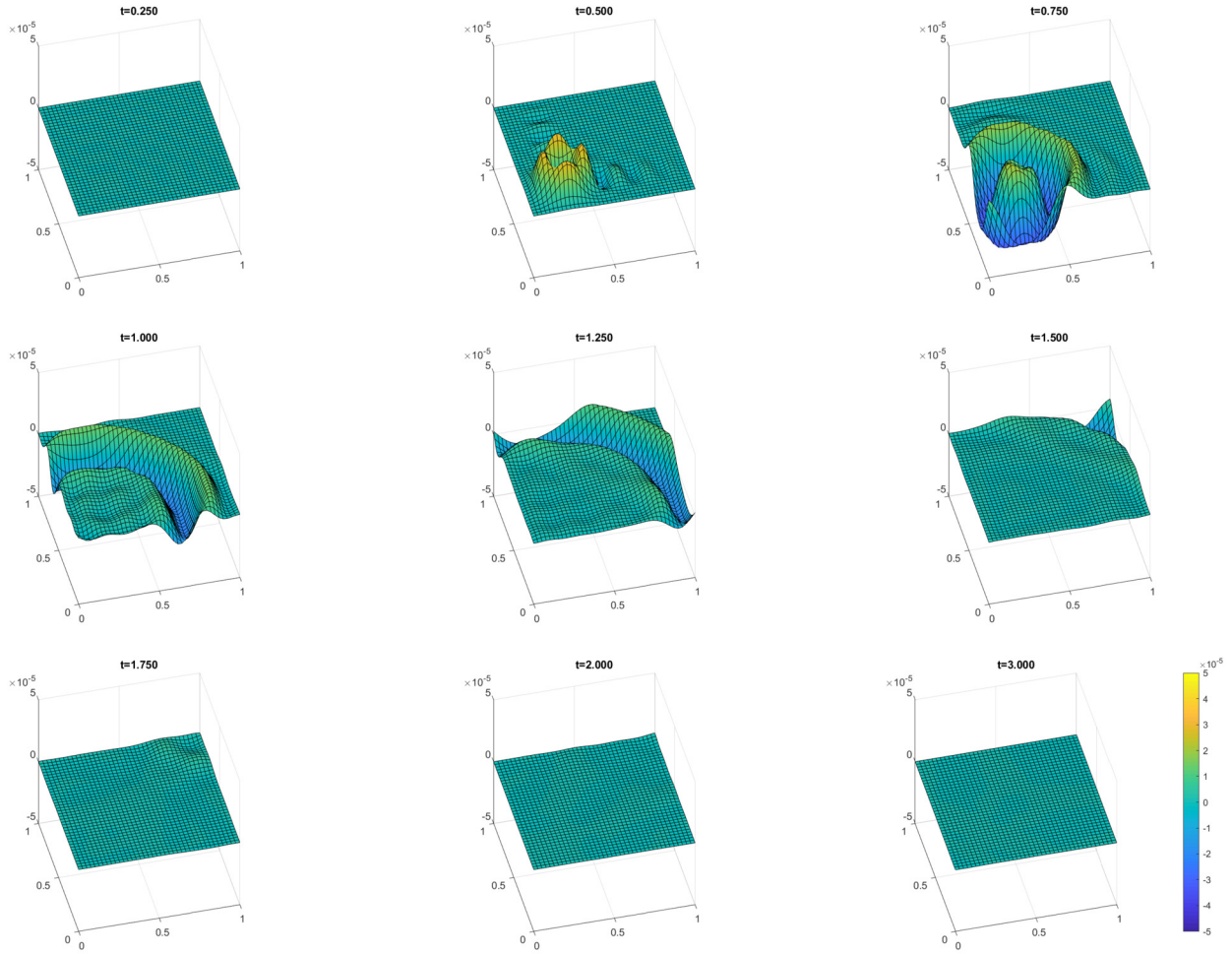

Fig. 6. Snapshots of one Ricker wavelet propagating from one corner of a square domain at nine time instants of the interval $[0, 3]$. IGA-Gal with $p = 6$, $k = 5$, $1/h = 10$, $\Delta t = 0.0005$.

5. Conclusions

In this paper, we have compared the Galerkin and Collocation Isogeometric approximations of the acoustic wave equation with absorbing boundary conditions, whereas the time discretization is based on second-order Newmark schemes. We have carried out an experimental investigation on the properties of the two IGA methods, focusing on their stability thresholds, convergence errors, accuracy, computational time, and sparsity of the stiffness matrices as functions of polynomial degree p, mesh size h, regularity k, and time step Δt. Besides more standard tests on stability thresholds and error convergence, we have focused on the comparison of the two IGA methods on two significant test problems in the framework of wave propagation simulations: the first problem concerns the accuracy of the IGA solutions with respect to an oscillatory exact solution having increasing wave number, while in the second problem we have compared the dissipation of two interfering Ricker wavelets by computing the energy L_2-norm of the numerical solution as a function of time. Despite the lack of theoretical results in the literature, numerical results show that the IGA Collocation method retains convergence and stability properties analogous to the IGA Galerkin method. In addition, we can conclude that in all tests IGA Collocation method is in general less accurate if we adopt the same choices of parameters p, k, h, and Δt. Nevertheless, regarding the computational cost and the amount of memory required to achieve a given accuracy, we observe that the IGA Collocation method often outperforms the IGA Galerkin method, especially when we consider the case of maximal regularity $k = p - 1$ with increasing NURBS degree p.

Limitations and future work. This study was limited to the acoustic wave equation in the reference square, but we conjecture that similar results hold for three dimensional domains. Given the tensor product structure of IGA domains and basis functions, we do not expect new technical issue.

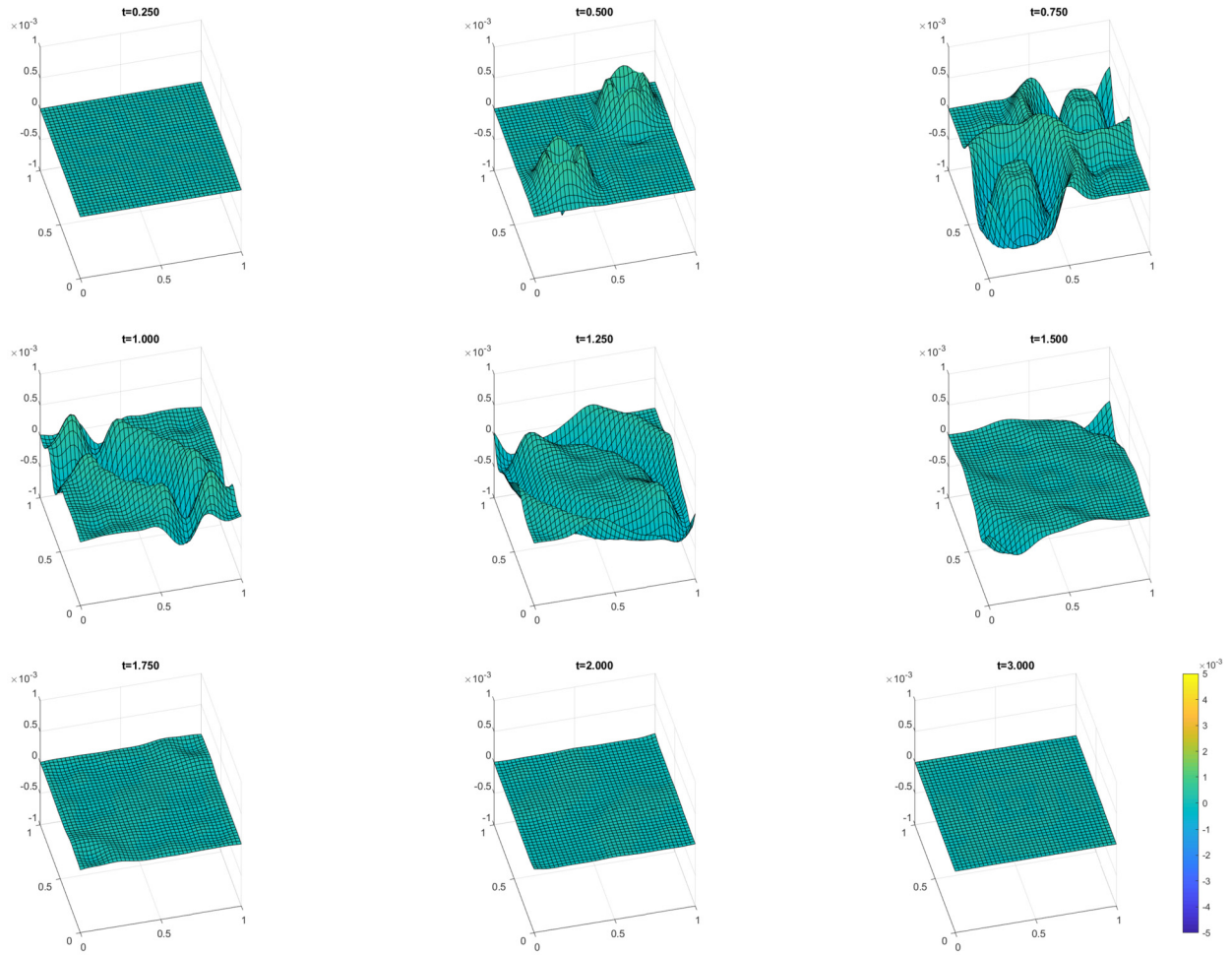

Fig. 7. Snapshots of two Ricker wavelets propagating from two corners of a square domain at nine time instants of the interval $[0, 3]$. IGA-Col with $p = 6,\ k = 5,\ 1/h = 10,\ \Delta t = 0.0005$.

This study was also confined to single-patch domains. Therefore additional study should be necessary in order to investigate the effects of inter-patch continuity conditions on both IGA Newmark discretizations considered in this paper. In this regard, the extension of efficient IGA approximations to multi-patch geometries is still an active research area, see e.g. [7].

In future work, we plan to construct efficient preconditioners for the linear systems arising at each time step of IGA Newmark schemes, as well as their extension to the three-dimensional case and to elastic wave problems. Additional extensions of our work include different time advancing schemes for the approximation of time derivatives and alternative choices of isogeometric collocation points, which hold the potential to enhance the accuracy and efficiency of our isogeometric simulations.

Declaration of competing interest

The authors declare that they have no conflict of interest.

References

[1] C. Anitescu, J. Yue, Y.J. Zhang, T. Rabczuk, An isogeometric collocation method using superconvergent points, Comput. Methods Appl. Mech. Eng. 284 (2015) 1073–1097.
[2] F. Auricchio, L. Beirão da Veiga, T.J.R. Hughes, A. Reali, G. Sangalli, Isogeometric collocation methods, Math. Models Methods Appl. Sci. 20 (11) (2010) 2075–2107.
[3] F. Auricchio, L. Beirão da Veiga, T.J.R. Hughes, A. Reali, G. Sangalli, Isogeometric collocation for elastostatics and explicit dynamics, Comput. Methods Appl. Mech. Eng. 249–252 (2012) 2–14.
[4] Y. Bazilevs, L. Beirão da Veiga, J.A. Cottrell, T.J.R. Hughes, G. Sangalli, Isogeometric analysis: approximation, stability and error estimates for h-refined meshes, Math. Models Methods Appl. Sci. 16 (2006) 1–60.
[5] P. Behnoudfara, G. Loli, A. Reali, G. Sangalli, V.M. Calo, Explicit high-order generalized-α methods for isogeometric analysis of structural dynamics, Comput. Methods Appl. Mech. Eng. 389 (2023) 114344.

[6] L. Beirão da Veiga, A. Buffa, G. Sangalli, R. Vazquez, Mathematical analysis of variational isogeometric methods, Acta Numer. 23 (2014) 157–287.
[7] M. Bosy, M. Montardini, G. Sangalli, M. Tani, A domain decomposition method for isogeometric multi-patch problems with inexact local solvers, Comput. Methods Appl. Mech. Eng. 80 (11) (2020) 2604–2621.
[8] R. Clayton, B. Engquist, Absorbing boundary conditions for acoustic and elastic wave equations, Bull. Seismol. Soc. Am. 67 (6) (1977) 1529–1540.
[9] J.A. Cottrell, T.J.R. Hughes, Y. Bazilevs, Isogeometric Analysis. Towards Integration of CAD and FEA, Wiley, 2009.
[10] J. Cottrell, A. Reali, Y. Bazilevs, T.J.R. Hughes, Isogeometric analysis of structural vibrations, Comput. Methods Appl. Mech. Eng. 195 (2006) 5257–5296.
[11] L. Dedé, C. Jäggli, A. Quarteroni, Isogeometric numerical dispersion analysis for two-dimensional elastic wave propagation, Comput. Methods Appl. Mech. Eng. 284 (2015) 320–348.
[12] C. De Falco, A. Reali, R. Vazquez, GeoPDEs: a research tool for isogeometric analysis of PDEs, Adv. Eng. Softw. 42 (12) (2011) 1020–1034.
[13] C. de Boor, A Practical Guide to Splines, Springer, 2001.
[14] S. Demko, On the existence of interpolation projectors onto spline spaces, J. Approx. Theory 43 (1985) 151–156.
[15] B. Engquist, A. Majda, Radiation boundary conditions for acoustic and elastic wave equations, Commun. Pure Appl. Math. 32 (1979) 313–357.
[16] J.A. Evans, R.R. Hiemstra, T.J.R. Hughes, A. Reali, Explicit higher-order accurate isogeometric collocation methods for structural dynamics, Comput. Methods Appl. Mech. Eng. 338 (15) (2018) 208–240.
[17] P. Gervasio, L. Dedé, O. Chanon, A. Quarteroni, A computational comparison between isogeometric analysis and spectral element methods: accuracy and spectral properties, J. Sci. Comput. 83 (2020) 1–45.
[18] D. Givoli, Non-reflecting boundary conditions, J. Comput. Phys. 94 (1) (1991) 1–29.
[19] H. Gomez, L. De Lorenzis, The variational collocation method, Comput. Methods Appl. Mech. Eng. 309 (2016) 152–181.
[20] T.J.R. Hughes, J.A. Cottrell, Y. Bazilevs, Isogeometric analysis: CAD, finite elements, NURBS, exact geometry, and mesh refinement, Comput. Methods Appl. Mech. Eng. 194 (2005) 4135–4195.
[21] T.J.R. Hughes, A. Reali, G. Sangalli, Isogeometric methods in structural dynamics and wave propagation, in: M. Papadrakakis, et al. (Eds.), COMPDYN 2009, 2009.
[22] F. Ihlenburg, Finite Element Analysis of Acoustic Scattering, Applied Mathematical Sciences, vol. 132, Springer-Verlag, Berlin, 1998.
[23] M.C. Junger, D. Feit, Sound, Structures and Their Interaction, MIT Press, Cambridge, MA, 1986.
[24] G. Loli, G. Sangalli, M. Tani, Easy and efficient preconditioning of the isogeometric mass matrix, Comput. Math. Appl. 116 (2022) 245–264.
[25] C. Manni, E. Sande, H. Speleers, Application of optimal spline subspaces for the removal of spurious outliers in isogeometric discretizations, Comput. Methods Appl. Mech. Eng. 389 (2022) 114260.
[26] M. Montardini, G. Sangalli, L. Tamellini, Optimal-order isogeometric collocation at Galerkin superconvergent points, Comput. Methods Appl. Mech. Eng. 316 (2017) 741–757.
[27] G. Mur, Absorbing boundary conditions for the finite–difference approximation of the time-domain electromagnetic–field equations, IEEE Trans. Electromagn. Compat. 23 (4) (1981) 377–382.
[28] N.M. Newmark, A method of computation for structural dynamics, Proc. ASCE, J. Eng. Mech. (EM3) 85 (1959) 67–94.
[29] A. Quarteroni, A. Tagliani, E. Zampieri, Generalized Galerkin approximations of elastic waves with absorbing boundary conditions, Comput. Methods Appl. Mech. Eng. 163 (1998) 323–341.
[30] J. Ren, H. Lin, A survey on isogeometric collocation methods with applications, Mathematics 11 (469) (2023) 323–341.
[31] L.L. Schumaker, Spline Functions: Basic Theory, 3rd edition, Cambridge Mathematical Library, Cambridge University Press, Cambridge, 2007.
[32] D. Schillinger, J.A. Evans, A. Reali, M.A. Scott, T.J.R. Hughes, Isogeometric collocation: cost comparison with Galerkin methods and extension to adaptive hierarchical NURBS discretizations, Comput. Methods Appl. Mech. Eng. 267 (2013) 170–232.
[33] R. Vazquez, A new design for the implementation of isogeometric analysis in Octave and Matlab: GeoPDEs 3.0, IMATI REPORT Series 16-02, 2016.
[34] W.L. Wood, A further look at newmark, houbolt, etc., time-stepping formulae, Int. J. Numer. Methods Eng. 20 (1984) 1009–1017.
[35] W.L. Wood, Practical Time-Stepping Schemes, Clarendon Press, Oxford, 1990.
[36] E. Zampieri, L.F. Pavarino, Explicit second order isogeometric discretizations for acoustic wave problems, Comput. Methods Appl. Mech. Eng. 348 (2019) 776–795.
[37] E. Zampieri, L.F. Pavarino, Isogeometric collocation discretizations for acoustic wave problems, Comput. Methods Appl. Mech. Eng. 385 (2021) 114047.